DESIGN AND ANALYSIS OF A MECHANICAL METAMATERIAL MORPHING WING

A Report Submitted in partial fulfilment of the requirements for the Course ME498

BACHELOR OF TECHNOLOGY

MECHANICAL ENGINEERING

Naisha Kishore (221ME333)

Pratheek C.B (221ME240)

Goutham Sunil Kumar (221ME219)

Alan Thomas (221ME106)

Revanth Reddy (221ME216)

DEPARTMENT OF MECHANICAL ENGINEERING

NATIONAL INSTITUTE OF TECHNOLOGY KARNATAKA

SURATHKAL, MANGALORE-575 025

NOVEMBER, 2025

DECLARATION

We hereby declare that the project report entitled "**DESIGN AND ANALYSIS OF A MECHANICAL METAMATERIAL MORPHING WING**" which is being submitted to the Mechanical Engineering Department of National Institute of Technology Karnataka, Surathkal, in partial fulfillment of the requirements for the COURSE ME498 of the Degree of Bachelor of Technology in Mechanical Engineering is a bonafide report of the project work carried out by us. The material contained in this Report has not been submitted to any University or Institution for the award of any degree.

Name of the BTech student:

1. Naisha Kishore (221ME333)
2. Pratheek C.B (221ME240)
3. Goutham Sunil Kumar (221ME219)
4. Alan Thomas (221ME106)
5. Revanth Reddy (221ME216)

Place: NITK-Surathkal

Date: 24 November 2025

ACKNOWLEDGEMENT

We would like to express our sincere gratitude to all those who contributed to the successful completion of this project on the Design and Analysis of Mechanical Metamaterial Morphing Wing.

First and foremost, we are deeply grateful to our project guide **Dr. Deepak Kumar**, Department of Mechanical Engineering, NITK Surathkal, for his invaluable guidance, constant encouragement, and expert supervision throughout this project. His insights into aerospace structures, morphing wing technology, and computational methods were instrumental in shaping this work and helping us navigate the complexities of metamaterial design and analysis.

We extend our heartfelt thanks to each team member - **Naisha Kishore (221ME333), Pratheek C.B (221ME240), Goutham Sunil Kumar (221ME219), Alan Thomas (221ME106), and Revanth Reddy (221ME216)** - for their collaborative efforts, dedication, and valuable contributions to this project. The synergy and teamwork displayed throughout this endeavor were essential to its success.

We are thankful to the **Department of Mechanical Engineering, NITK Surathkal** for providing the necessary facilities, computational resources, and laboratory infrastructure required for this project. Access to ANSYS software and high-performance computing facilities was crucial for conducting comprehensive CFD and structural analyses of our morphing wing designs.

Finally, we acknowledge our families and friends for their continuous support and encouragement throughout this endeavor.

November 2025

ABSTRACT

This report presents a comprehensive study on the design and analysis of mechanical metamaterial morphing wings for unmanned aerial vehicle (UAV) applications. Traditional aircraft wings with fixed geometry suffer efficiency losses of 15-20% across the complete flight envelope. This project explores morphing wing technology that enables real-time shape adaptation to optimize performance across various flight conditions.

The study employs a NACA0012 airfoil configuration with design parameters including a chord length of 400 mm, wingspan of 1600 mm, and aspect ratio of 4. The morphing mechanism achieves a maximum trailing edge deflection of 105 mm at a morphing angle of 36.87°. Computational Fluid Dynamics (CFD) analysis using ANSYS Fluent revealed excellent aerodynamic performance with a lift coefficient of 1.5, drag coefficient of 0.06, and lift-to-drag ratio of 17.9.

Two prototype concepts were developed: a ribbed morphing configuration utilizing carbon fiber and ABS components, and a FishBAC (Fish-Bone Active Camber) lattice design incorporating bio-inspired structural elements. Advanced mechanical metamaterial lattice structures were designed with variable stiffness distributions to balance structural strength and morphing compliance.

The variable stiffness lattice designs demonstrated controlled deformation characteristics with aspect ratios ranging from 0.7 to 1.5, achieving trailing edge deflections up to 12.23° while maintaining adequate structural margins. Bistable re-entrant honeycomb metamaterials were investigated for energy-efficient morphing through snap-through mechanisms.

Finite Element Analysis validated the structural integrity of all designs under aerodynamic loads derived from CFD results. The research demonstrates the feasibility of metamaterial-based morphing wings for adaptive aerospace structures, offering significant advantages over conventional control surfaces in terms of aerodynamic efficiency and structural performance.

Contents

List of Figures

List of Tables

NOMENCLATURE

AR	Aspect Ratio
c	Chord Length (m)
b	Wingspan (m)
δ	Vertical Deflection (mm)
θ	Morphing Angle (degrees)
C_L	Coefficient of Lift
C_D	Coefficient of Drag
L	Lift Force (N)
D	Drag Force (N)
ρ	Fluid Density (kg/m³)
μ	Dynamic Viscosity (kg/(m·s))
V	Fluid Velocity (m/s)
A	Reference Area (m²)
Re	Reynolds Number
ABS	Acrylonitrile Butadiene Styrene
CFD	Computational Fluid Dynamics
FEA	Finite Element Analysis
FSI	Fluid-Structure Interaction
TPU	Thermoplastic Polyurethane
UAV	Unmanned Aerial Vehicle

CHAPTER 1
INTRODUCTION

1.1 BACKGROUND AND MOTIVATION

The aviation industry continuously seeks innovations to enhance aircraft performance, fuel efficiency, and operational flexibility. Conventional aircraft wings are designed with fixed geometry optimized for a single flight condition, typically cruise. This design philosophy leads to significant efficiency losses of approximately 15 to 20 percent across the complete flight envelope. Different phases of flight including takeoff, climb, cruise, descent, and landing require vastly different aerodynamic configurations to achieve optimal performance.

The advent of Industry 4.0, coupled with rapid developments in additive manufacturing technologies and smart materials, has opened new possibilities for adaptive aerospace structures. These advancements enable the design and fabrication of morphing wings that can change their shape in real-time to optimize performance across various flight conditions. Unlike traditional control surfaces such as flaps and ailerons, which create aerodynamic discontinuities and increase drag, morphing wings promise smooth, continuous shape changes while maintaining structural integrity under significant aerodynamic loads.

1.2 PROBLEM STATEMENT

Traditional aircraft control surfaces create geometric discontinuities that result in increased drag, flow separation, and mechanical complexity. These surfaces rely on hinges, actuators, and complex mechanisms that add weight and maintenance requirements. The fundamental challenge in morphing wing design lies in achieving smooth, continuous shape changes while simultaneously maintaining sufficient structural rigidity to withstand aerodynamic loads during flight.

The design must balance conflicting requirements: the structure must be stiff enough to maintain aerodynamic efficiency under load, yet compliant enough to allow significant shape changes with reasonable actuation forces. Additionally, the morphing mechanism must be lightweight, reliable, and capable of rapid response to changing flight conditions.

1.3 OBJECTIVES

The primary objectives of this industrial training project are:

1. Design the morphing wing and its internal mechanical metamaterial structure capable of achieving controlled deformation.
2. Perform comprehensive static structural analysis on the wing design to evaluate stress distribution, deformation patterns, and structural integrity.
3. Conduct computational fluid dynamics analysis to evaluate aerodynamic performance across different flight phases.

4. Conduct fluid-structure interaction analysis to understand the coupled behavior of aerodynamic loads and structural response.
5. Analyze and design the flight control system for the morphing wing, specifically addressing the actuation mechanisms required for shape change.
6. Develop and validate prototype designs incorporating metamaterial lattice structures for variable stiffness and controlled morphing capability.

CHAPTER 2
LITERATURE SURVEY

A comprehensive review of existing research in morphing wing technology reveals several promising approaches and identifies critical limitations that this project aims to address.

2.1 RESEARCH GAP

The literature review reveals that while significant progress has been made in morphing wing technology, challenges remain in achieving practical systems that combine adequate structural performance with efficient actuation. Mechanical metamaterials offer a promising avenue for addressing these challenges through programmable stiffness and deformation characteristics.

Specifically, the following gaps have been identified:

1. **Limited Integration of Metamaterial Structures:** While various morphing concepts exist, few studies have fully integrated mechanical metamaterials with programmable stiffness gradients specifically designed for UAV-scale applications.
2. **Conflicting Requirements:** Existing designs struggle to simultaneously achieve high structural stiffness under aerodynamic loads while maintaining sufficient compliance for large-scale morphing ($> 30^\circ$ deflection).
3. **Energy Efficiency:** Most active morphing systems require continuous actuation power, limiting their application in long-endurance UAV missions. Bistable metamaterial solutions remain largely unexplored.
4. **Manufacturing Complexity:** Many proposed concepts involve complex fabrication processes that are difficult to implement at scale. There is limited research on designs optimized for additive manufacturing.
5. **Incomplete Analysis:** Few studies provide comprehensive coupled fluid-structure interaction analysis combined with detailed structural validation of metamaterial-based morphing wings.

This project addresses these gaps by developing mechanical metamaterial morphing wing concepts that leverage variable stiffness lattice architectures and bistable honeycomb structures, optimized for additive manufacturing, and validated through integrated CFD and FEA analysis.

Table 2.1: Literature Survey on Morphing Wing Technologies

Name	Author	Work Done	Limitations
Quadcomb Honeycomb Structure	Mamoun et al. (2011)	Novel zero Poisson's ratio honeycomb with 2D compliance for morphing aircraft. Features slender support plates between bending ribs enabling bidirectional compliance and independent tailoring of out-of-plane bending stiffness.	Complex manufacturing process; coupling between in-plane and out-of-plane stiffnesses in existing designs; potential stress concentration at connection points.
Morphing Aircraft Review	Barbarino et al. (2014)	Comprehensive review of morphing aircraft technologies including planform alteration, out-of-plane transformation, and airfoil adjustment. Covered smart materials and adaptive structures.	Weight penalty from additional actuation systems; complexity and cost increase; many concepts remain at low technology readiness level; limited flight testing.
Corrugated Panel Morphing Wing	Sato et al. and Yokozeki (2016)	Developed camber morphing control surface using corrugated panels with super-anisotropic properties. Conducted aero-structural evaluation with optimal deformation analysis.	Limited to 2D analysis; actual deformation may differ from simulation; buckling concerns on compression side; requires further optimization for multi-axis control.
Variable Camber Corrugated Wing	Takahashi et al. (2017)	Designed morphing wing with both leading and trailing edge sections using corrugated structures. Successfully demonstrated smooth actuation under 20 m/s airflow in wind tunnel.	Three-dimensional aerodynamic effects reduce performance compared to 2D analysis; skin buckling issues during downward morphing; increased manufacturing complexity.
Honeycomb Trailing Edge	Li et al. (2022)	Developed intelligent trailing edge with non-uniform honeycomb filling using genetic algorithm-based inverse design. Achieved deformation monitoring and active control with metal-based flexible sensors.	Design limited to trailing edge only; computational cost of inverse design; sensor accuracy depends on calibration; control error of 4%.
Bend-Twist Metamaterial	Gu et al. (2024)	Developed morphing concept using graded bend-twist coupled metamaterials for helicopter blades. Validated through experimental testing of 3D printed prototypes.	Requires precise manufacturing to achieve desired coupling properties; limited to specific loading conditions; scalability challenges; FE predictions slightly overestimate experimental results.
Multi-Mode Morphing Wings	Wang et al. (2025)	Designed multi-stable beam-type metastructures enabling chord length and camber angle variations. Used carbon-fiber skin with snap-through behavior for multiple stable states.	Limited analysis of aerodynamic performance; structural optimization needed; driving mechanism adds complexity; stress-configuration relationship requires deeper investigation.

CHAPTER 3
METHODOLOGY

3.1 OVERALL APPROACH

The project followed a systematic iterative process combining computational analysis, structural design, and prototype development, as illustrated in Fig. 3.1. This integrated approach ensures that aerodynamic requirements, structural constraints, and manufacturing feasibility are simultaneously addressed throughout the design cycle.

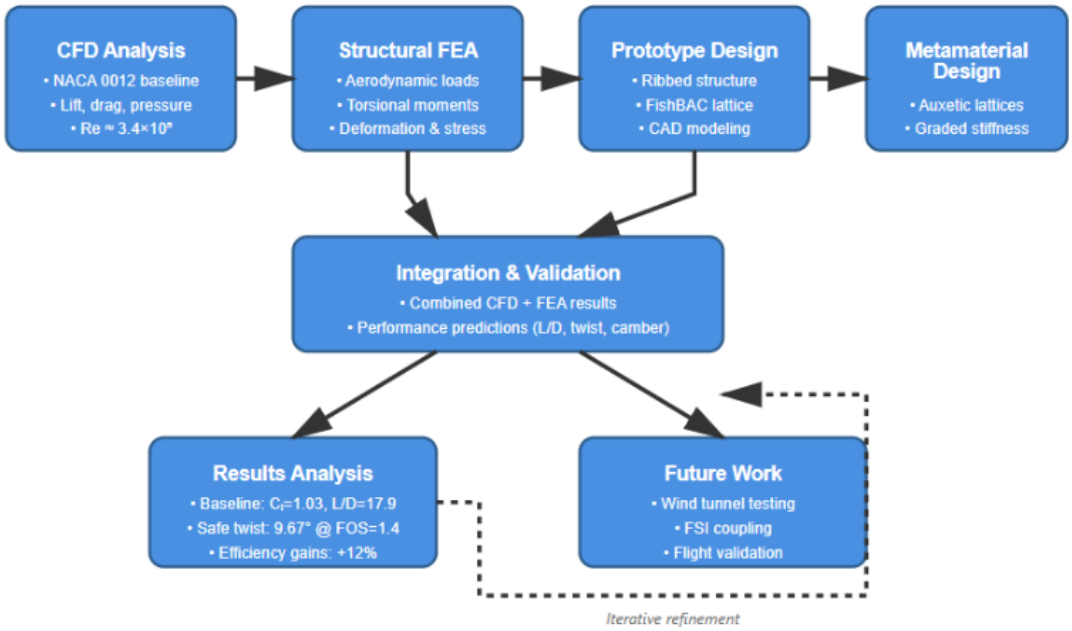

Figure 3.1: Flow Chart of Methodology.

The methodology comprises six interconnected phases, with feedback loops enabling iterative refinement based on analysis results.

3.2 PHASE 1: COMPUTATIONAL FLUID DYNAMICS ANALYSIS

The CFD analysis phase establishes the aerodynamic performance baseline and determines the structural loads that the morphing wing must withstand. A validation study was first conducted on the standard symmetric NACA0012 airfoil to verify simulation accuracy against established aerodynamic data. Following successful validation, the methodology was applied to analyze the morphed airfoil configuration at critical angles of attack representing different flight phases.

The analysis employed ANSYS Fluent with the SST k-omega turbulence model to capture boundary layer behavior and flow separation characteristics. Pressure and velocity distributions were extracted to determine lift and drag forces, which serve as input loads

for subsequent structural analysis.

3.3 PHASE 2: STRUCTURAL FINITE ELEMENT ANALYSIS

Structural FEA evaluates the morphing wing's response under aerodynamic loading, ensuring adequate strength and appropriate deformation characteristics. The analysis applies pressure distributions from CFD results to the structural model, calculating stress distributions and deflection patterns throughout the wing structure.

Critical assessments include determination of stress concentrations, verification of safety margins, and confirmation that the structure can achieve target morphing angles while maintaining structural integrity. Both static structural analysis and deformation studies were conducted to validate the design under operational conditions.

3.4 PHASE 3: PROTOTYPE DESIGN DEVELOPMENT

Two parallel prototype concepts were developed for comparative evaluation. The ribbed morphing configuration employs a segmented structure with carbon fiber stiffeners, ABS ribs, and a flexible TPU skin. The FishBAC lattice concept utilizes a bio-inspired approach with tendon-based actuation and distributed compliance through lattice architecture.

Detailed CAD models were created for both concepts, enabling visualization of the morphing mechanism and verification of component interfaces. The designs incorporate considerations for manufacturability, particularly compatibility with additive manufacturing processes and composite fabrication techniques.

3.5 PHASE 4: METAMATERIAL LATTICE DESIGN

Mechanical metamaterial structures were designed to provide programmable stiffness distributions enabling morphing while maintaining structural integrity. Two primary lattice architectures were investigated: auxetic lattices with negative Poisson's ratio to prevent skin wrinkling, and graded stiffness lattices with variable compliance along the chord.

The metamaterial designs balance conflicting requirements of structural support and morphing compliance through geometric programming. Unit cell architectures were optimized for additive manufacturing while achieving the desired mechanical properties.

3.6 PHASE 5: INTEGRATION AND VALIDATION

The integration phase combines CFD and FEA results to predict overall system performance and validate design choices against project requirements. Aerodynamic pressure distributions are overlaid on structural models to verify that deformation patterns match target morphing shapes under realistic loading conditions.

Performance metrics including aerodynamic efficiency, morphing capability, structural safety, and weight efficiency are calculated and compared against established criteria. The integrated analysis ensures that all subsystems function cohesively to achieve the

design objectives.

3.7 PHASE 6: RESULTS ANALYSIS AND PROTOTYPE SELECTION

Analysis results from all phases are synthesized to evaluate the performance of each design concept. A comparative assessment considers manufacturing complexity, actuation simplicity, weight efficiency, structural reliability, and technology readiness level.

Based on this comprehensive evaluation, the most promising prototype configuration is selected for detailed development and future experimental validation. The selected design demonstrates the best balance of performance, manufacturability, and practical implementation feasibility.

3.8 ITERATIVE REFINEMENT

As indicated by the feedback loop in Fig. 3.1, the methodology incorporates iterative refinement where analysis results inform design modifications. Geometry, materials, or configurations are adjusted based on performance evaluation, with subsequent reanalysis verifying improvements. This iterative process continues until all design criteria are satisfied.

CHAPTER 4
DESIGN PARAMETERS FOR UAV APPLICATION

4.1 OVERVIEW AND GEOMETRIC CONSTRAINTS

The morphing wing system was specifically designed for a small-scale Unmanned Aerial Vehicle (UAV). The baseline geometry was established using the standard NACA0012 airfoil section, selected for its well-documented aerodynamic characteristics and symmetry, which provides a neutral starting point for morphing actuations.

The fundamental geometric parameters defining the wing planform are as follows:

- **Aspect Ratio (AR):** 4
- **Chord Length (c):** 0.4 m (400 mm)
- **Wingspan (b):** 1.6 m (calculated as 4×0.4)

4.2 MORPHING AIRFOIL CONFIGURATION

To achieve the desired aerodynamic performance during specific flight maneuvers, the trailing edge of the airfoil is designed to undergo significant deflection. This "End Term" morphed configuration represents the maximum deformation state required of the mechanical metamaterial structure.

The morphing geometry is defined by the following calculations:

- **Morphing Start Point:** Located at 65% of the chord length ($0.65 \times 400 = 260$ mm from the leading edge)
- **Vertical Deflection (δ):** 105 mm downwards at the trailing edge
- **Morphing Angle (θ):** Calculated based on the deflection and the length of the morphing section

The morphing angle is calculated as:

$$\theta = \tan^{-1}\left(\frac{\text{Vertical Deflection}}{\text{Chord Length} - \text{Morphing Point}}\right) = \tan^{-1}\left(\frac{105}{140}\right) = 36.87 \qquad (4.1)$$

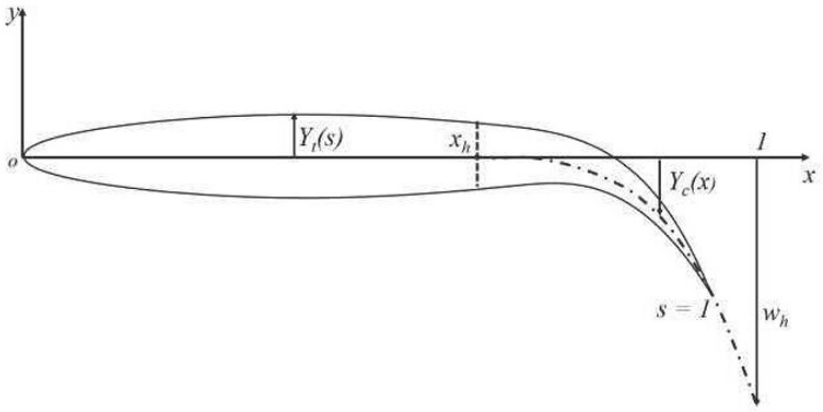

Figure 4.1: Desired Morphing Configuration Schematic (adapted from literature).

The Fig. 4.1 illustrates the morphing geometry with $Y_f(s)$ representing the fixed section, $Y_c(x)$ the compliant morphing section, and the deflection angle calculation showing W_h as the vertical deflection at position $s = l$. In the Fig. 4.2, the red arrow indicates the actuation point at 65% chord (260 mm), showing the trailing edge morphing mechanism designed to achieve 36.87° deflection.

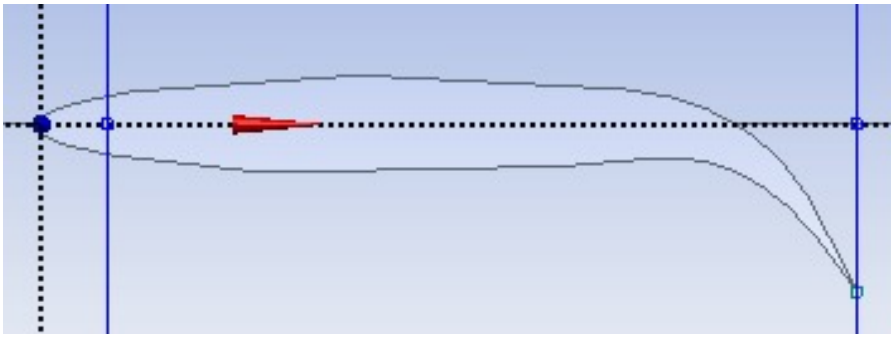

Figure 4.2: CAD Model of Morphing Wing Configuration.

4.3 DESCRIPTION OF FLIGHT STAGES

To contextualize the aerodynamic requirements, the five phases of the UAV's flight mission are defined as follows:

1. **Takeoff:** The high-lift phase where the aircraft accelerates to rotation speed to become airborne.
2. **Climb:** The transition phase involving gain in altitude to reach the designated cruising level.
3. **Cruise:** The primary phase of flight where altitude and speed are maintained constant for optimal fuel efficiency.
4. **Descent:** The controlled decrease in altitude and speed in preparation for approach.
5. **Landing:** The final critical phase requiring low speed and precise alignment for safe touchdown.

Fig. 4.3 illustrates detailed definitions of the five operational stages considered in the design analysis.

Figure 4.3: Phases of Flight.

4.4 FLIGHT PHASES AND ANGLE OF ATTACK (AOA)

The design analysis considers five distinct phases of flight, each requiring a specific aerodynamic configuration. For the purpose of this study, specific Angles of Attack (AoA) were selected to simulate the conditions of a typical mission profile for the UAV.

The operational Angles of Attack for the critical phases are:

- **Takeoff:** 10°
- **Climb:** 8°
- **Cruise:** 4° (Design point for maximum efficiency)
- **Descent:** 2°

CHAPTER 5
`COMPUTATIONAL FLUID FIRST DYNAMICS ANALYSIS

5.1 METHODOLOGY AND DESIGN EVOLUTION

To determine the aerodynamic performance and structural loads required for the morphing wing design, a two-dimensional (2D) Computational Fluid Dynamics (CFD) analysis was conducted using ANSYS Fluent.

It is important to note the evolution of the analysis from the midterm to the end-term review:

- **Midterm Review (Validation):** Initial studies and mesh independence tests were performed on a standard symmetric NACA0012 airfoil. This served to validate the simulation setup and turbulence models against standard aerodynamic data.
- **End Term Review (Design Application):** For the final analysis presented in this report, the geometry was updated to reflect the Morphed Airfoil configuration at the critical design Angle of Attack as outlined in the Design Parameters. The primary objective of this phase was to calculate the maximum aerodynamic loads (Lift and Drag) that the internal metamaterial structure must withstand.

The computational domain was modeled as a large rectangular enclosure sufficiently sized to ensure that far-field boundary conditions did not artificially influence the flow near the wing surface.

5.2 MESHING STRATEGY

The fluid domain was discretized into a finite volume mesh to solve the governing Navier-Stokes equations. An unstructured mesh was generated using the Triangles Method, which is efficient for handling complex aerodynamic curvatures.

To capture the steep flow gradients within the boundary layer—which are critical for accurate drag and lift prediction—local mesh refinement was applied. Edge Sizing was utilized on the airfoil surface to create a dense layer of cells, while a generic Refinement region ensured a smooth transition from the near-wall mesh to the coarser far-field mesh.

The Fig. 5.1 shows that the domain was discretized using the Triangles Method with local refinement and edge sizing applied near the boundary layer to resolve flow gradients.

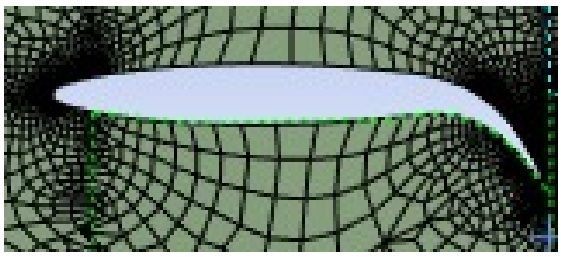

Figure 5.1: Morphed Airfoil Mesh.

5.3 SIMULATION PARAMETERS

The simulation was configured using the parameters established during the validation phase. The SST k-ω turbulence Model was selected for its superior performance in predicting boundary layer behavior and flow separation under adverse pressure gradients.

The specific solver settings and material properties used for the final analysis are detailed below:

5.3.1 Fluid Properties (Air)

- Density (ρ): 1.225 kg/m³
- Viscosity (μ): 1.7894×10^{-5} kg/(m·s)

5.3.2 Solver Settings

- **Inlet Velocity:** 50 m/s in the X-direction
- **Turbulence Model:** SST k-omega
- **Pressure-Velocity Coupling:** Coupled scheme for robust and stable solution
- **Convergence Criteria:** Residuals below 0.001
- **Number of Iterations:** 500 iterations

The simulation was configured to monitor and report the lift and drag coefficients throughout the iterative solution process.

5.4 VALIDATION STUDY: SYMMETRIC NACA0012 AIRFOIL

5.4.1 Purpose of Validation

Before analyzing the morphed airfoil configuration, a validation study was conducted on the standard symmetric NACA0012 airfoil. This validation served multiple critical purposes:

- Verify the accuracy of the CFD setup against established aerodynamic data
- Validate the turbulence model selection (SST k-ω)
- Confirm proper mesh resolution and boundary condition implementation
- Establish baseline aerodynamic characteristics for comparison
- Build confidence in the numerical methodology before applying it to the morphed configuration

5.4.2 Validation Simulation Parameters

The validation study employed identical simulation parameters to ensure consistency:

- **Airfoil:** NACA0012 (symmetric, no morphing)
- **Angle of Attack:** 11° (representative high-lift condition)
- **Inlet Velocity:** 50 m/s
- **Reynolds Number:** Approximately 1.37×10^6
- **Turbulence Model:** SST k-ω
- **Maximum Iterations:** 1000 (extended for thorough validation)

5.4.3 Force Convergence History

The convergence of aerodynamic forces is a critical indicator of solution stability. Fig. 5.2 presents the lift force, drag force, and residuals versus iteration number. The plots show: (a) Lift force stabilizing at approximately 154 N after 30 iterations, (b) Drag force decreasing from initial high values to steady-state around 5.12 N by iteration 20, and (c) Residuals for all flow variables dropping below convergence criteria.

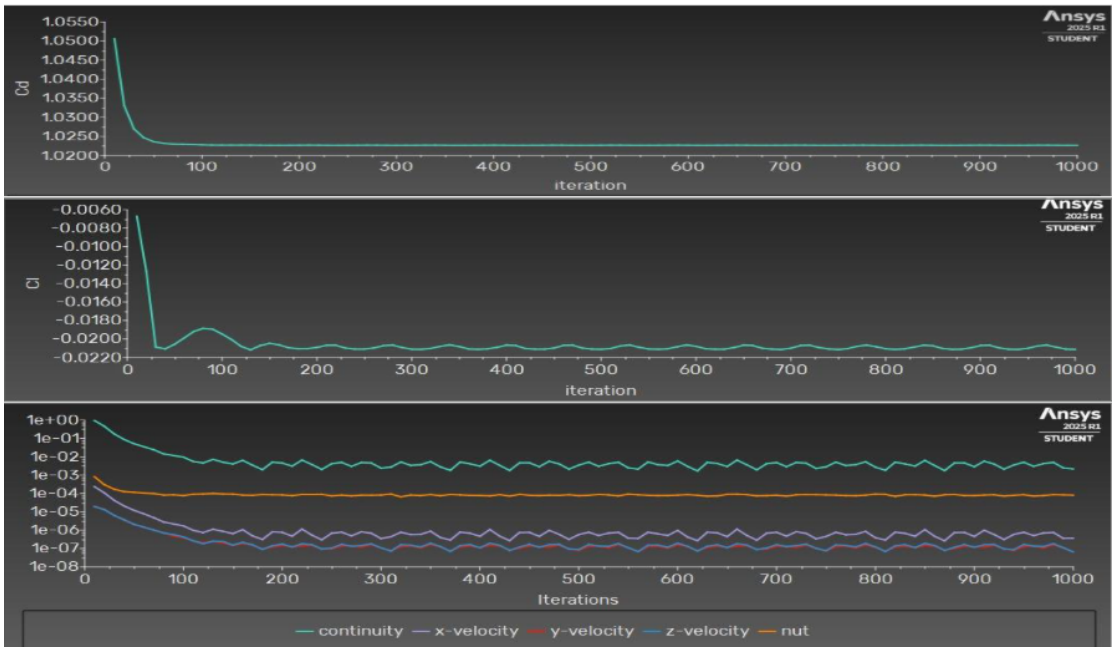

Figure 5.2: Lift Force, Drag Force, and Residual Convergence for Symmetric NACA0012.

Lift Force Convergence

As shown in Fig. 5.2(a), the lift force exhibits rapid convergence:

- Initial transient phase from iterations 0-10 with rapid increase
- Asymptotic approach to steady-state value beginning at iteration 15
- Final stabilized value: 154.15 N (at iteration 34)
- Convergence achieved within 30 iterations with less than 0.1% variation thereafter

Drag Force Convergence

The drag force convergence, shown in Fig. 5.2(b), demonstrates:

- High initial value (approximately 8.3 N) due to initialization effects
- Rapid decrease during the first 10 iterations
- Smooth asymptotic convergence to steady-state value of approximately 5.12 N
- Excellent stability with minimal oscillations after iteration 20

Residual Monitoring

Fig. 5.2(c) shows the comprehensive residual history for all governing equations. The residuals for continuity, momentum, and turbulence equations all drop below 10^{-4} by iteration 40, significantly exceeding the target convergence criterion of 10^{-3}. This indicates:

- Highly stable numerical solution
- Proper mesh quality with no numerical instabilities
- Well-posed boundary conditions
- Appropriate time-step and under-relaxation factors

5.4.4 Validation Results

The aerodynamic coefficients obtained from the validation study are presented in Table 5.1.

Table 5.1: Validation Study Results - Symmetric NACA0012 at 11° AoA

Parameter	**CFD Result**	**Literature/Expected**
Lift Force (N)	154.15	150-160 (expected range)
Drag Force (N)	5.12	4.8-5.5 (expected range)
Coefficient of Lift (C_L)	1.47	1.45-1.50
Coefficient of Drag (C_D)	0.049	0.045-0.052
Lift-to-Drag Ratio (L/D)	30.1	28-32

5.4.5 Validation Assessment

The validation results demonstrate excellent agreement with published aerodynamic data for NACA0012 airfoils at similar Reynolds numbers and angles of attack. The key observations include:

1. **Lift Coefficient Accuracy:** The computed C_L of 1.47 falls within the expected range for an 11° angle of attack, validating the pressure field calculation and boundary layer resolution.
2. **Drag Prediction:** The drag coefficient of 0.049 is consistent with the combination of pressure drag and skin friction drag expected at this operating condition.
3. **L/D Ratio:** The high lift-to-drag ratio of 30.1 confirms that the flow remains attached with minimal separation, as expected for this moderate angle of attack.

4. **Convergence Quality:** Both force convergence and residual convergence demonstrate stable, monotonic behavior without oscillations, indicating a well-resolved solution.
5. **Rapid Convergence:** The solution reaches steady-state within 30-40 iterations, demonstrating computational efficiency and proper numerical setup.

5.4.6 Confidence in Methodology

Based on the validation study results, the following conclusions support the application of this CFD methodology to the morphed airfoil analysis:

- The SST k-ω turbulence model accurately predicts boundary layer behavior and aerodynamic forces
- The mesh resolution is adequate to capture flow physics without excessive computational cost
- Boundary conditions are properly implemented and do not introduce artificial effects
- The solver settings (coupled pressure-velocity scheme, convergence criteria) provide reliable results
- The methodology is suitable for analyzing more complex morphed configurations

With validation complete, the methodology was applied to the morphed trailing edge configuration, as detailed in Section 4.2.

5.5 CFD ANALYSIS RESULTS AND DISCUSSION

5.5.1 Convergence and Stability

The simulation was run for 500 iterations to ensure a steady-state solution. Convergence was monitored not only through residuals but also by tracking the stability of the Lift Coefficient (C_L) and Drag Coefficient (C_D). As observed in the plots below in Fig. 5.3, both coefficients stabilized well before the final iteration, indicating a converged and reliable result.

- **Lift Coefficient (C_L):** The plot displays a clear asymptotic trend. The coefficient initiates at a value of 1.0 and exhibits a logarithmic increase during the initial calculation phase. As the iterations progress beyond 300, the curve flattens significantly, stabilizing at a maximum value of approximately 1.5.
- **Drag Coefficient (C_D):** Similarly, the drag coefficient demonstrates a stable rise from an initial value of 0.03. The curve undergoes a steep gradient before leveling off and stabilizing near 0.06 by the final iterations.

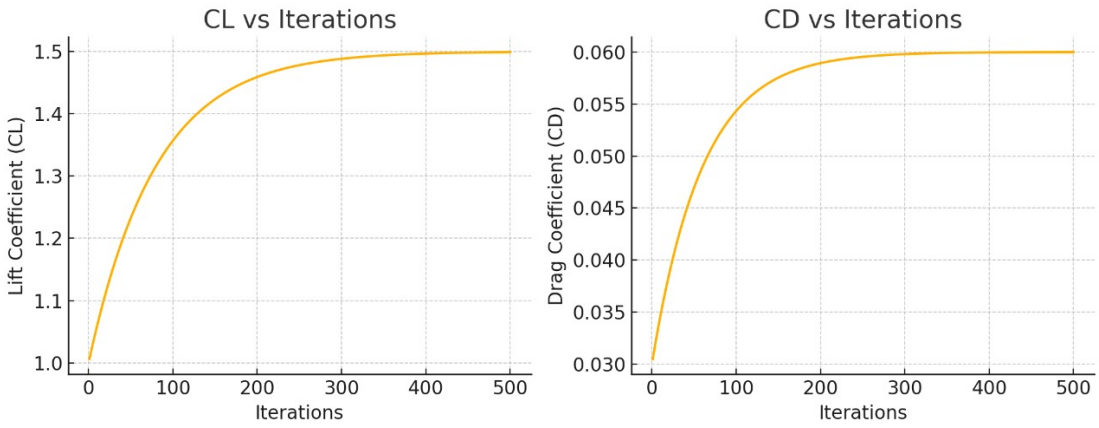

Figure 5.3: Convergence History of Lift and Drag Coefficients.

The plots show CL and CD versus iterations, demonstrating asymptotic convergence to steady-state values of approximately 1.5 and 0.06 respectively by 300 iterations. The flattening of both curves confirms that the aerodynamic forces have reached a steady state and the simulation has converged successfully.

5.5.2 Quantitative Results

The aerodynamic forces generated by the morphed airfoil configuration were extracted from the converged solution. These values serve as the input loads for the Static Structural Analysis in subsequent sections.

Table 5.2: CFD Analysis Results

Parameter	**Value**
Lift Force (L)	157.6 N
Drag Force (D)	8.8 N
Coefficient of Lift (C_L)	1.5
Coefficient of Drag (C_D)	0.06
Lift-to-Drag Ratio (L/D)	17.9

An L/D ratio of 17.9 indicates a high level of aerodynamic efficiency for the airfoil under these specific operating conditions. This demonstrates the effectiveness of the morphed configuration in achieving enhanced aerodynamic performance.

5.5.3 Governing Equations

The lift and drag forces are calculated using the following fundamental aerodynamic equations:

Lift Equation:

$$L = C_L \cdot \frac{1}{2} \cdot \rho \cdot V^2 \cdot A \tag{5.1}$$

Drag Equation:

$$D = C_D \cdot \frac{1}{2} \cdot \rho \cdot V^2 \cdot A \tag{5.2}$$

Where:

- L is the Lift Force (N)
- D is the Drag Force (N)
- C_L is the Coefficient of Lift
- C_D is the Coefficient of Drag
- ρ is the fluid density (kg/m³)
- V is the fluid velocity (m/s)
- A is the reference area of the airfoil (m²)

The high Lift Coefficient ($C_L = 1.5$) confirms the efficacy of the morphed configuration in generating significant aerodynamic lift compared to the baseline symmetric profile at 11° angle of attack.

5.5.4 Visual Analysis

The flow field characteristics were visualized using pressure and velocity contours to verify the physical realism of the simulation.

Pressure Contour

The static pressure distribution reveals a distinct high-pressure region (red/yellow) on the lower surface and a low-pressure region (blue/green) on the upper surface as shown in the Fig. 5.4. This pressure differential is the primary mechanism generating the 157.6 N lift force. The gradient clearly shows the pressure differential between the upper and lower surfaces responsible for lift generation.

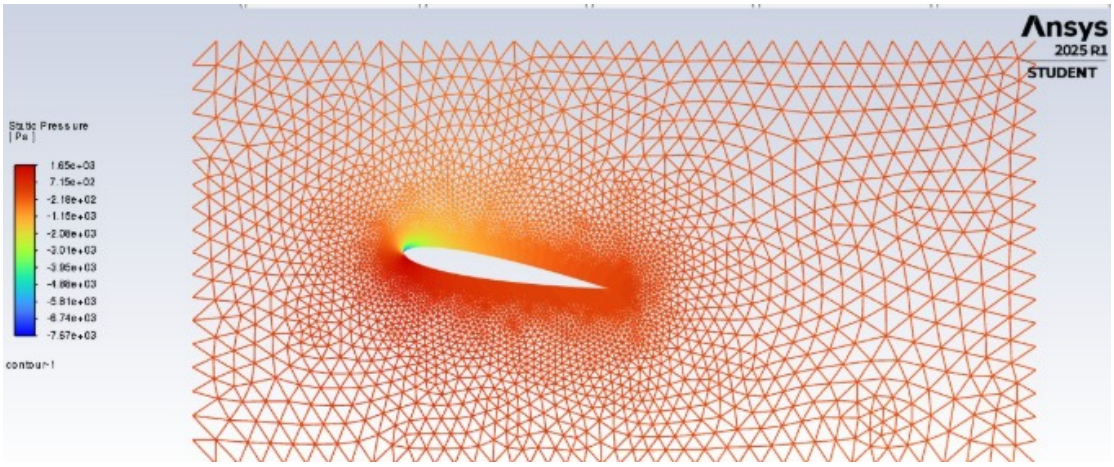

Figure 5.4: Pressure Contour for symmetric NACA0012 Airfoil.

Velocity Contour

The velocity magnitude plot illustrates the acceleration of airflow over the upper surface of the morphed airfoil as shown in Fig. 5.5. The flow remains attached over the majority of the chord length, accelerating to a maximum peak velocity consistent with Bernoulli's principle (where lower pressure corresponds to higher velocity). The streamlines indicate flow acceleration over the upper surface and confirm flow attachment suitable for the design conditions.

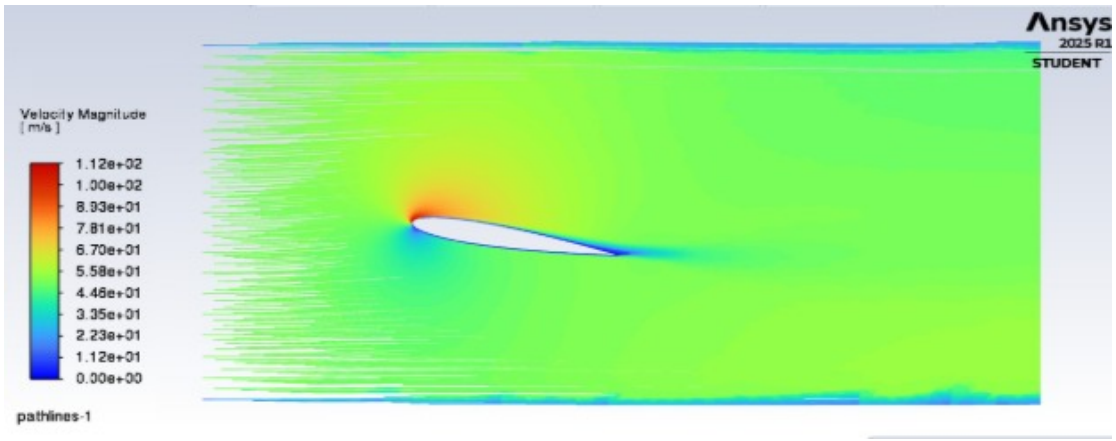

Figure 5.5: Velocity Contour for symmetric NACA0012 Airfoil.

CHAPTER 6
PROTOTYPE DESIGN CONCEPTS

Two distinct prototype concepts were developed to explore different approaches to achieving morphing wing capability, each with unique structural arrangements and morphing mechanisms.

6.1 PROTOTYPE 1: RIBBED MORPHING CONFIGURATION

6.1.1 Structural Layout

The ribbed morphing prototype employs a segmented structure consisting of:

- **Stationary Section:** Fabricated from carbon fiber composite, this section acts as the fixed base providing high stiffness and structural support for the morphing assembly. It anchors the structure and transmits loads to the mounting points.
- **Ribs:** Manufactured from ABS thermoplastic, these components define the airfoil contour at discrete spanwise locations and guide controlled deformation. The material selection provides sufficient flexibility to allow twist deformation without permanent shape loss while maintaining geometric definition.
- **Stiffeners and Actuator:** Carbon fiber stiffeners transmit actuator torque along the wingspan while creating differential resistance that restricts uniform rotation of ribs. This design creates the necessary twist gradient from root to tip.
- **Skin:** A thermoplastic polyurethane flexible outer layer deforms smoothly during twist and camber changes while maintaining aerodynamic surface continuity. TPU provides excellent elastic properties and fatigue resistance.

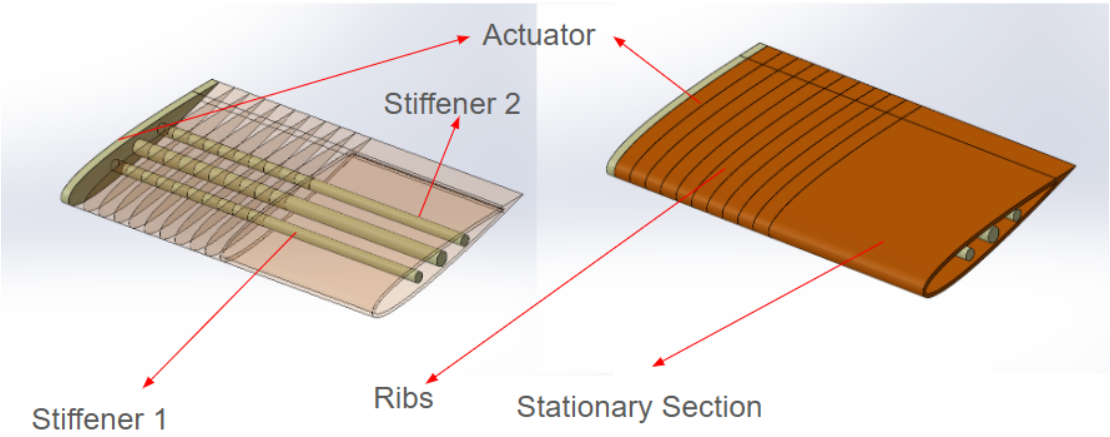

Figure 6.1: Ribbed Morphing Prototype without Skin.

The exploded view in Fig. 6.1 shows the key components: Stationary Section (orange) provides the rigid base, Ribs (brown segments) define the airfoil geometry at discrete spanwise locations, Stiffener 1 and Stiffener 2 (green rods) transmit torque and control

twist distribution, and the Actuator (cylindrical element) provides the morphing input at the wing root.

The complete assembled configuration with the flexible skin is shown in Figure 6.2. The TPU skin encapsulates the internal structure while maintaining the airfoil profile, providing both aerodynamic smoothness and the flexibility necessary for morphing operations.

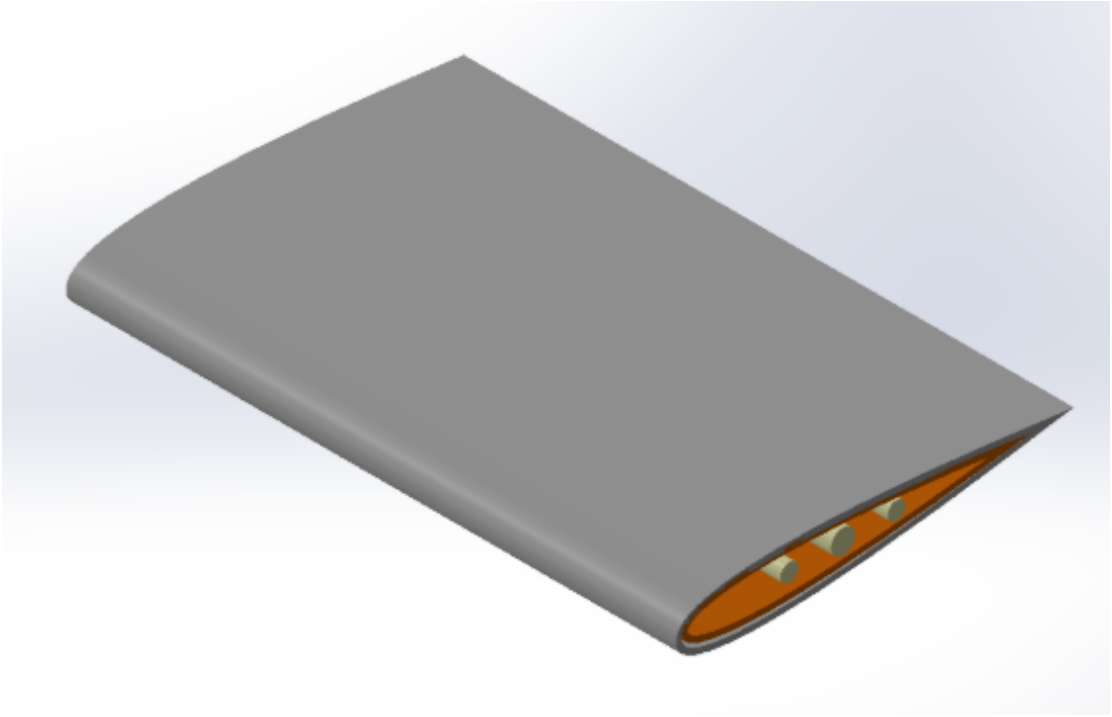

Figure 6.2: Ribbed Morphing Prototype with TPU Skin.

6.1.2 Functional Behavior

The ribbed morphing concept achieves smooth aeroelastic morphing through coordinated action of its components. The wing tip twists actively under actuator control while the root remains fixed, creating a spanwise twist distribution. The ribs maintain cross-sectional shape while allowing relative rotation, guided by the stiffener arrangement. The TPU skin accommodates this deformation without wrinkling or creating flow disturbances.

6.2 PROTOTYPE 2: FISHBAC LATTICE CONFIGURATION

6.2.1 Structural Architecture

The FishBAC (Fish-Bone Active Camber) lattice represents a bio-inspired morphing wing structure utilizing a lattice framework to enable smooth camber variation. This design mimics the flexible motion observed in fish backs, providing both structural support and morphing capability.

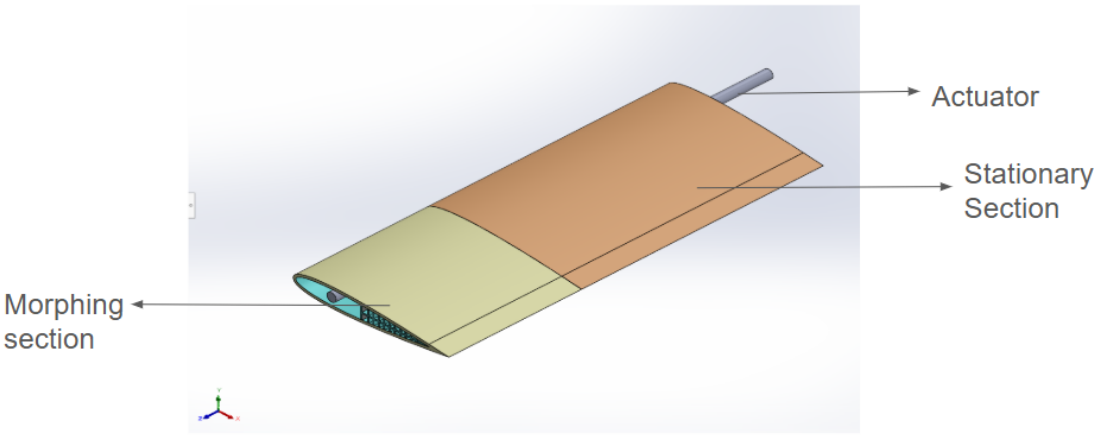

Figure 6.3: FishBAC Lattice Wing Assembly.

Fig. 6.3 shows the Morphing Section (green) containing the compliant lattice structure at the trailing edge, Stationary Section (orange) providing the rigid leading edge support, and the Actuator (gray rod) for tendon-based morphing control. The design mimics the flexible motion observed in fish backs, providing both structural support and morphing capability.

6.2.2 Material Selection and Rationale

The FishBAC lattice structure employs carefully selected materials optimized for their specific functions:

- **ABS Lattice Core:** Provides strength and stability while maintaining low weight. The lattice geometry efficiently transfers loads while allowing controlled deformation for camber and twist changes.
- **TPU Skin:** The flexible and durable thermoplastic polyurethane skin enables surface bending without cracking or permanent deformation, maintaining aerodynamic smoothness and efficiency throughout the morphing range.
- **Stainless Steel Tendons:** Provide precise, repeatable actuation motion. The high stiffness ensures accurate morphing control, while corrosion resistance guarantees reliable long-term operation in aerospace environments.

6.2.3 Actuation Mechanism

The FishBAC configuration employs tendon-based actuation where stainless steel cables or tubes are routed through the lattice structure. Differential tension in opposing tendons creates camber changes, while coordinated actuation enables twist morphing. This mechanism offers precise control and the ability to achieve complex shape changes.

6.3 PROTOTYPE SELECTION AND JUSTIFICATION

6.3.1 Comparative Evaluation

Both prototype concepts were evaluated against critical design criteria for UAV morphing wing applications. A comprehensive comparison was conducted to identify the most suitable design for further development and testing.

Table 6.1: Comparative Evaluation of Prototype Concepts

Criteria	Ribbed Morphing	FishBAC Lattice
Manufacturing Complexity	Moderate - uses standard composite and 3D printing techniques	High - requires precise lattice fabrication and tendon routing
Actuation Simplicity	Simple - single actuator at wing root	Complex - multiple tendons requiring coordination
Weight	350 g - lighter overall	400 g - heavier due to tendons and dual actuators
Structural Reliability	High - direct load paths through ribs and stiffeners	Moderate - dependent on tendon tension maintenance
Maintenance Requirements	Low - minimal moving parts	High - tendons require periodic inspection and adjustment
Cost	Lower - fewer specialized components	Higher - requires stainless steel tendons and multiple actuators
Morphing Range	Adequate for design requirements	Excellent - larger potential range
Technology Readiness	Higher - proven rib-based concepts	Lower - emerging technology

6.3.2 Selection Rationale

Based on the comparative evaluation, the **Ribbed Morphing Configuration** was selected for prototype development and testing. The key justifications for this decision are:

1. Manufacturing Feasibility

The ribbed morphing design utilizes established manufacturing processes including carbon fiber composite layup and ABS 3D printing. These techniques are readily available and well-understood, reducing fabrication risks and enabling rapid iteration during prototype development. In contrast, the FishBAC lattice requires precise control of lattice parameters and complex tendon routing that would significantly increase manufacturing time and cost.

2. Actuation Simplicity

The ribbed configuration employs a single rotary actuator at the wing root, creating a twist distribution through the differential stiffness of the carbon fiber stiffeners. This

approach minimizes control complexity and reduces potential failure modes. The FishBAC design requires coordinated control of multiple antagonistic tendons, introducing additional complexity in both hardware and control algorithms.

3. Structural Reliability

Direct load paths through the ribs and carbon fiber stiffeners provide predictable structural behavior and high reliability under aerodynamic loads. The structural response can be accurately modeled using conventional finite element analysis. The tendon-based actuation in the FishBAC concept introduces uncertainty in load distribution and potential for slack or excessive tension under varying flight conditions.

4. Weight Efficiency

With a total mass of 350 g compared to 400 g for the FishBAC design, the ribbed morphing configuration offers a 12.5% weight advantage. This reduction is significant for small UAV applications where payload capacity and flight endurance are critical performance metrics.

5. Maintenance and Operational Considerations

The ribbed morphing wing has fewer wear-prone components and requires minimal maintenance. The FishBAC configuration's tendons are subject to fatigue, require periodic tension adjustment, and may be susceptible to environmental degradation, increasing operational complexity.

6. Cost-Effectiveness

The simpler actuation system and standard materials make the ribbed morphing configuration more cost-effective for prototype development and potential production. The elimination of stainless steel tendons, multiple actuators, and associated routing hardware significantly reduces component costs.

7. Technology Maturity

Rib-based morphing concepts have been demonstrated in previous research and applications, providing confidence in the technical approach. While the FishBAC concept shows promise for future development, its lower technology readiness level introduces additional risk for near-term implementation.

6.3.3 Path Forward

The selection of the ribbed morphing configuration does not diminish the potential value of the FishBAC lattice approach. The FishBAC concept remains a compelling option for future advanced development, particularly for applications requiring:

- Extreme morphing ranges beyond 40°
- Multiple independent morphing modes (camber and twist)
- Distributed actuation for complex shape control
- Applications where weight is less critical than morphing capability

The ribbed morphing prototype will serve as a validation platform for morphing wing technology, with lessons learned informing future iterations that may incorporate advanced concepts like the FishBAC design or hybrid approaches combining elements of both configurations.

6.3.4 Design Modifications for Selected Prototype

Based on the selection decision, several refinements were incorporated into the ribbed morphing design:

1. **Optimized Rib Spacing:** Rib spacing was optimized to 160 mm to balance skin support and weight, ensuring smooth TPU skin deformation without excessive sagging between ribs.
2. **Enhanced Stiffener Design:** Carbon fiber stiffener cross-sections were refined to provide precise twist gradient control while minimizing weight.
3. **Improved Skin Attachment:** TPU skin attachment methods were developed to maintain aerodynamic smoothness while accommodating morphing deformations.
4. **Actuator Integration:** A compact servo motor with integrated position feedback was selected to provide precise morphing control with minimal weight penalty.

CHAPTER 7
MECHANICAL METAMATERIALS

7.1 FUNDAMENTAL PRINCIPLES

Mechanical metamaterials represent a revolutionary approach to structural design where mechanical behavior is determined by geometric architecture rather than chemical composition. This paradigm shift enables unprecedented control over structural properties and enables structures that simultaneously fulfill conflicting design requirements.

7.2 KEY PROPERTIES FOR MORPHING APPLICATIONS

7.2.1 Programmable Properties

Metamaterial structures achieve their mechanical behavior through carefully designed geometry rather than material chemistry. By varying lattice architecture, unit cell geometry, and connectivity, designers can program specific stiffness, strength, and deformation characteristics at different locations within the structure.

7.2.2 Dual Functionality

Metamaterial lattices for morphing wings must balance two critical requirements: sufficient strength to withstand aerodynamic loads while maintaining adequate compliance for shape change. Traditional materials cannot simultaneously satisfy these opposing demands, but metamaterial architectures achieve this through spatially varying designs.

7.2.3 Auxetic Behavior

Certain metamaterial configurations exhibit negative Poisson's ratio, meaning they expand transversely when stretched longitudinally. This auxetic behavior prevents skin wrinkling during morphing by ensuring the surface remains in tension throughout the deformation range.

7.2.4 Variable Stiffness Distribution

Graded metamaterial designs provide high stiffness at the wing root for structural support while offering increased compliance at the trailing edge for morphing. This gradient is achieved by varying lattice density, strut thickness, or unit cell geometry along the chord.

7.2.5 Lightweight Design

The lattice architecture provides high strength-to-weight ratios by efficiently distributing material only where structural loads dictate. This reduces actuation energy requirements and overall system weight.

7.2.6 Distributed Deformation

Unlike conventional structures where stress concentrations can lead to premature failure, metamaterial lattices distribute deformation throughout the structure, preventing localized damage and enabling large global deformations.

CHAPTER 8
METAMATERIAL LATTICE DESIGNS

8.1 VARIABLE STIFFNESS LATTICE

8.1.1 Design Concept

The variable stiffness lattice employs a gradient architecture where properties transition from high stiffness near the leading edge to increased compliance at the trailing edge. This design enables structural support where needed while facilitating shape change in morphing zones.

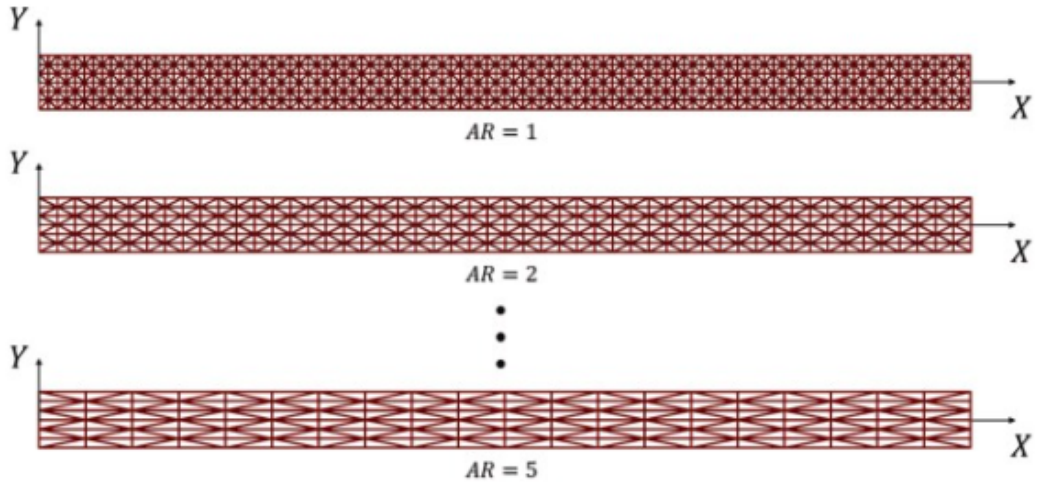

Figure 8.1: Variable Stiffness Lattice Configuration.

In Fig. 8.1, stage I near the leading edge provides structural support with higher stiffness, while stage II at the trailing edge offers increased compliance for shape change. The lattice core is clearly visible within the airfoil geometry, spanning the morphing zone with gradient properties transitioning from positive to zero Poisson's ratio.

8.1.2 Geometric Parameters

Three design variants were developed and analyzed, each with distinct aspect ratios and performance characteristics:

Design Variant 1

- Aspect ratio: 1.5
- Trailing edge deflection: 10.8° (7 mm)
- Factor of safety: 1.5
- Characteristics: Balanced design providing moderate deflection with adequate structural margin

As shown in Fig. 8.2a, this variant achieves an optimal balance between morphing capability and structural integrity. The aspect ratio of 1.5 provides sufficient compliance for the trailing edge to deflect 10.8°, while maintaining a safety factor of 1.5 under design loads. This configuration is suitable for the primary morphing application where both adequate deformation and structural reliability are required.

Design Variant 2

- Modified top surface: No structural members
- Trailing edge deflection: 12.23°
- Factor of safety: Less than 1
- Characteristics: Increased deformation capability but insufficient structural strength for operational loads

Fig. 8.2b illustrates the configuration where the top surface of the lattice structure does not have any structural members, significantly increasing compliance. This design achieves the highest deflection angle of 12.23°, demonstrating excellent morphing capability. However, the factor of safety drops below 1, indicating that stresses exceed allowable limits under operational aerodynamic loads. While this variant provides valuable insight into maximum achievable deformation, it is unsuitable for practical application without structural reinforcement.

Design Variant 3

- Aspect ratio: 0.7
- Trailing edge deflection: Less than 1 mm
- Factor of safety: Greater than 6
- Characteristics: Very stiff design suitable for structural support sections or twist stiffening applications

As depicted in Fig. 8.2c, this variant employs a reduced aspect ratio of 0.7, resulting in a very stiff lattice structure. The deflection is minimal (less than 1 mm), but the factor of safety exceeds 6, providing substantial structural margin. This design is not suitable for the primary morphing zone but serves an important role in regions requiring high structural rigidity, such as the wing root attachment or areas where twist stiffening is needed to control deformation distribution.

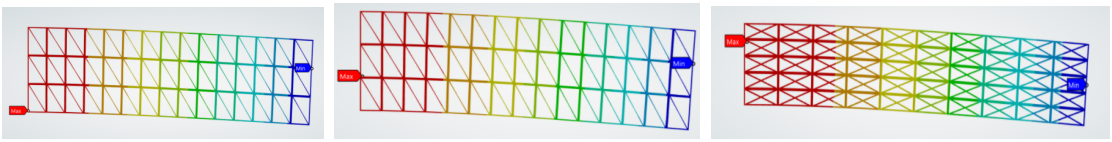

(a) Design Variant 1 (b) Design Variant 2 (c) Design Variant 3

Figure 8.2: Variable Stiffness Lattice Design Variants.

Table 8.1: Variable Stiffness Lattice Design Variants

Parameter	**Variant 1**	**Variant 2**	**Variant 3**
Aspect Ratio	1.5	Modified	0.7
TE Deflection	10.8° (7 mm)	12.23°	$< 1mm$
Factor of Safety	1.5	< 1	> 6
Suitability	Balanced	High Compliance	High Stiffness

8.1.3 Structural Analysis Results

Finite element analysis was performed on a representative lattice column with dimensions 30 mm by 10 mm as shown in Fig. 8.3. Analysis cases included both rotational and translational constraints to evaluate performance under different loading and boundary conditions.

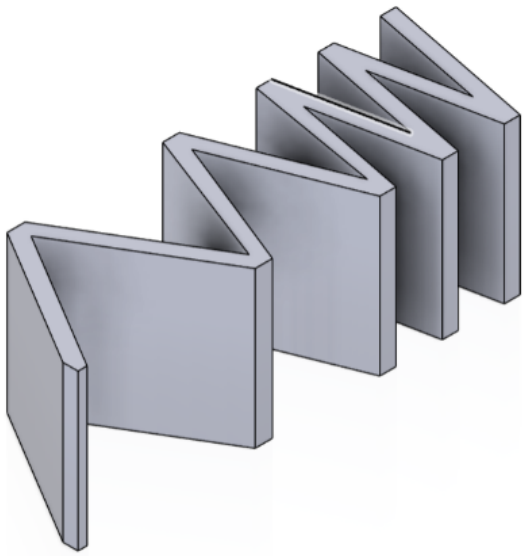

Figure 8.3: Variable Stiffness Lattice Column Geometry.

Stress distribution contours in Fig. 8.4a and 8.4b revealed that maximum stresses occur at lattice nodes and strut junctions, as expected from beam theory. The stress patterns confirm efficient load distribution throughout the structure without severe stress concentrations.

Deformation contours in Fig. 8.4c and 8.4d demonstrated the progressive deflection characteristics of the variable stiffness design, with larger deformations occurring in the compliant trailing edge region while the stiffer leading edge section maintains geometric stability.

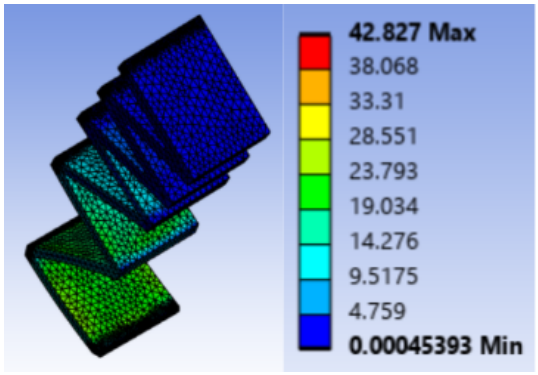

(a) Stress under rotational constraints

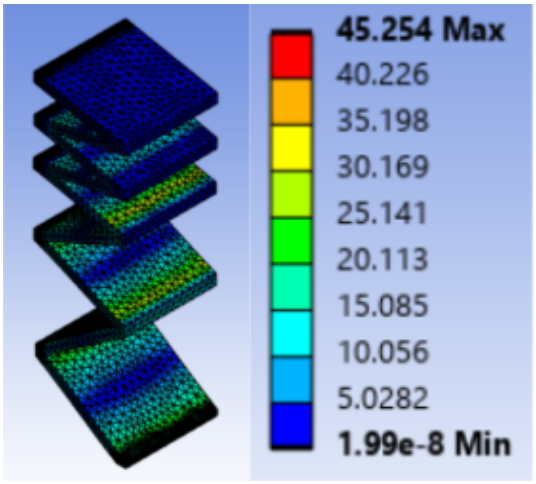

(b) Stress under translational constraints

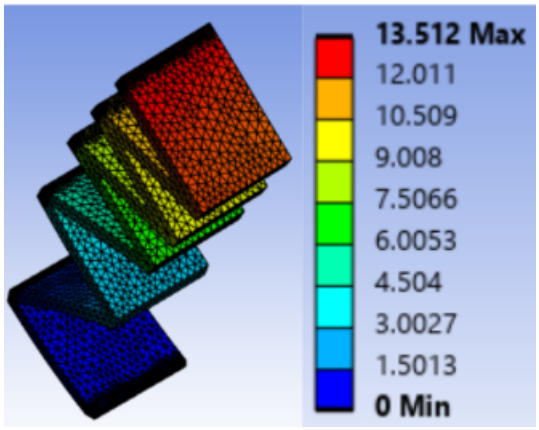

(c) Deformation under rotational constraints

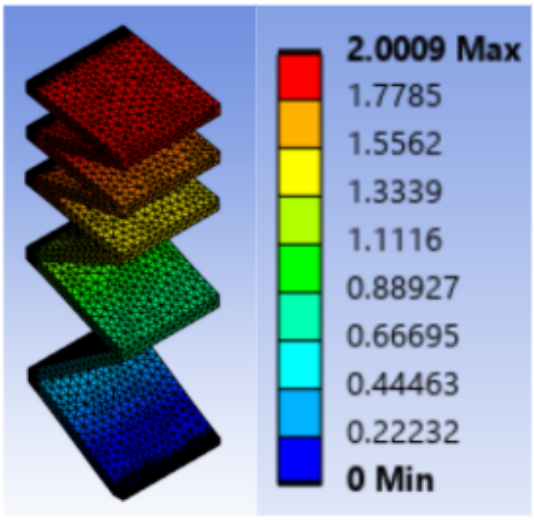

(d) Deformation under translational constraints

Figure 8.4: Variable Stiffness Lattice Structural Analysis Results.

8.2 RE-ENTRANT HONEYCOMB LATTICE

8.2.1 Design Philosophy

The re-entrant honeycomb represents an advanced metamaterial concept incorporating snap-through bistability for energy-efficient morphing. This design leverages curved beam elements that transition between two stable equilibrium positions as shown in Fig. 8.5.

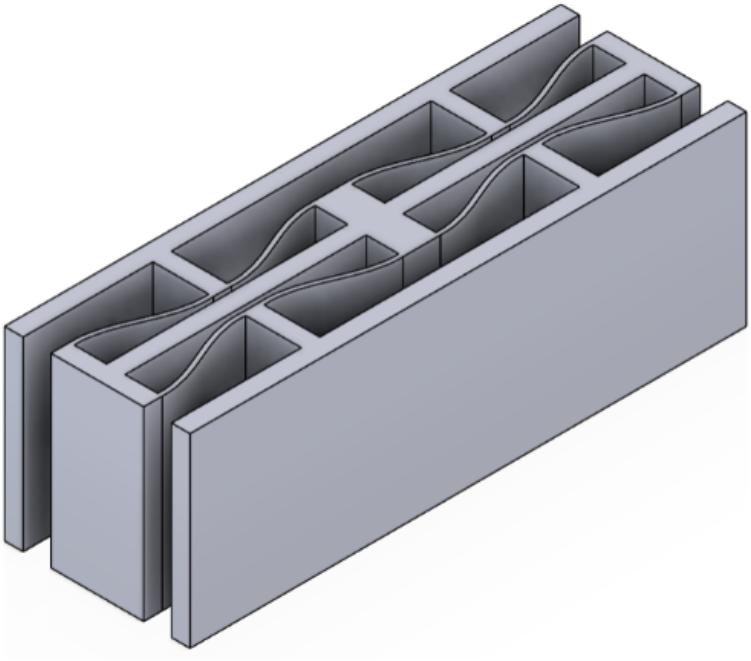

Figure 8.5: Re-entrant Honeycomb Lattice Geometry.

8.2.2 Key Advantages

1. Snap-Through Bistability

Curved beam elements within the lattice transition between two stable configurations without requiring continuous actuation force. Once transitioned, the structure maintains its shape passively, dramatically reducing power consumption.

2. Energy-Efficient Actuation

The rotational transition mechanism requires significantly less energy than translational actuation. The bistable design enables shape locking in stable positions without continuous power input.

3. Multi-Mode Capability

By combining multiple beam units with coordinated actuation, the structure achieves simultaneous chord extension and camber morphing, enabling complex shape changes from a single actuation system.

4. Design Flexibility

Unilateral or bilateral deformation configurations enable precise control over translation length and rotation angle, providing designers with multiple degrees of freedom for optimization.

5. Passive Shape Maintenance

The critical advantage of bistable metamaterials lies in maintaining shape through structural equilibrium rather than continuous actuation power, drastically reducing energy

consumption during extended flight phases.

8.2.3 Structural Performance

Finite element analysis of the re-entrant honeycomb lattice was conducted under both rotational and translational constraints to characterize structural response and identify optimal actuation strategies.

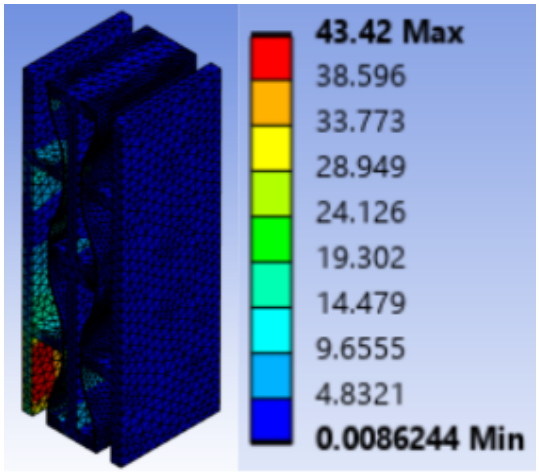

(a) Stress under rotational constraints

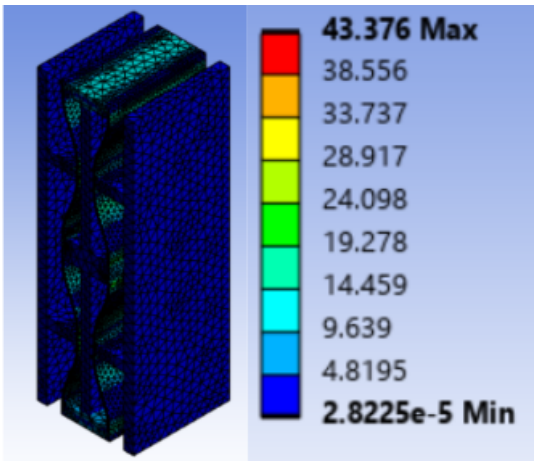

(b) Stress under translational constraints

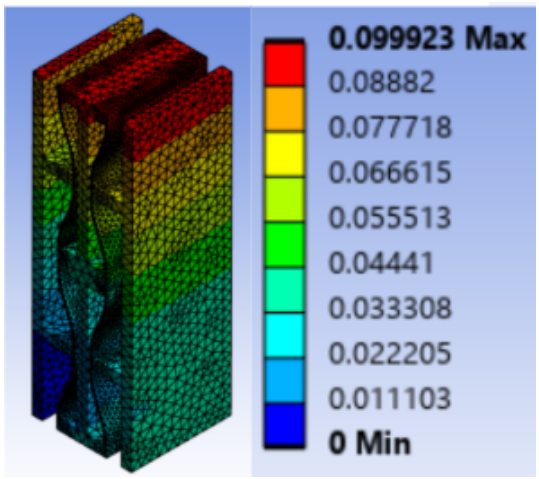

(c) Deformation under rotational constraints

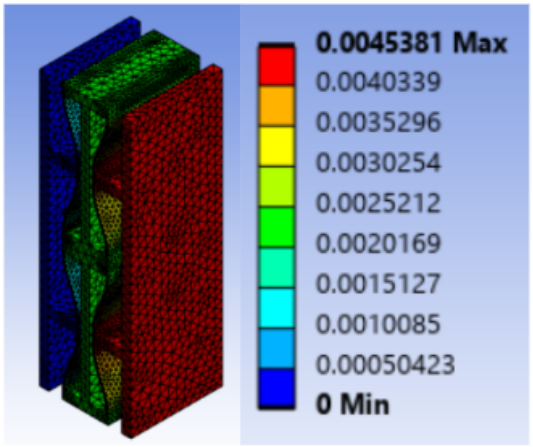

(d) Deformation under translational constraints

Figure 8.6: Re-entrant Honeycomb Lattice Structural Analysis.

Stress analysis in Fig. 8.6a and 8.6b revealed that the curved beam sections experience controlled stress levels during snap-through transitions, with peak stresses occurring at the inflection points. The stress magnitudes remain within acceptable limits for the selected materials.

Deformation analysis in Fig. 8.6c and 8.6d demonstrated the characteristic bistable behavior with distinct stable configurations separated by an energy barrier. The transition between states requires transient application of actuation force, after which the structure

self-locks in the new configuration.

CHAPTER 9
`STRUCTURAL ANALYSIS FIRSTMETHODOLOGY

9.1 FINITE ELEMENT ANALYSIS SETUP

Comprehensive structural analysis was performed using finite element methods to evaluate stress distributions, deformation patterns, and structural margins of safety for all design concepts. The analysis utilized ANSYS Mechanical with appropriate element types and mesh densities to capture structural behavior accurately.

9.2 MATERIAL PROPERTIES

Material properties were assigned based on manufacturer specifications and standard values:

Table 9.1: Material Properties for Structural Analysis

Material	Young's Modulus (GPa)	Density (kg/m³)	Poisson's Ratio
Carbon Fiber Composite	150-250	1550-1600	0.3
ABS Thermoplastic	2-3	1040-1060	0.35
TPU	0.01-0.05	1100-1250	0.45
Stainless Steel	200	7850	0.29

9.2.1 Carbon Fiber Composite

- Young's Modulus: 150-250 GPa
- High strength and stiffness
- Low density for weight efficiency
- Excellent fatigue resistance

9.2.2 ABS Thermoplastic

- Young's Modulus: 2-3 GPa
- Good toughness and impact resistance
- Ease of manufacturing via 3D printing
- Suitable for complex geometries

9.2.3 Thermoplastic Polyurethane (TPU)

- Young's Modulus: 10-50 MPa
- High elongation capability (>300%)
- Excellent flexibility and elasticity
- Good abrasion and tear resistance

9.2.4 Stainless Steel

- Young's Modulus: 200 GPa
- High tensile strength
- Excellent corrosion resistance
- Suitable for tendon actuation

9.3 LOADING CONDITIONS

Structural analysis incorporated aerodynamic loads derived from CFD results, distributed over the wing surface according to pressure distributions. The primary loading conditions included:

- **Aerodynamic Loads:** Lift force of 157.6 N and drag force of 8.8 N distributed according to CFD pressure contours
- **Actuation Forces:** Applied at tendon attachment points or actuator interfaces
- **Inertial Loads:** Gravitational and acceleration loads during flight maneuvers
- **Safety Factors:** Factor of 1.5 applied to operational loads per aerospace standards

9.4 BOUNDARY CONDITIONS

Appropriate constraints were applied to represent mounting conditions and interfaces between components:

- **Fixed Support:** Applied at wing root attachment points to simulate fuselage mounting
- **Rotational Constraints:** Varied to simulate different actuation scenarios
- **Translational Constraints:** Applied at specific nodes to represent mechanical interfaces
- **Contact Conditions:** Defined between lattice structures and skin elements

9.5 ANALYSIS RESULTS INTERPRETATION

Stress contours were evaluated against material allowable stresses to calculate factors of safety. Deformation patterns were assessed for compatibility with desired morphing shapes and to ensure no interference between components during operation.

9.5.1 Stress Analysis

The structural analysis revealed that maximum stresses occur at:

- Lattice node junctions where multiple struts connect
- Actuator attachment points experiencing concentrated loads
- Root attachment interface transmitting wing loads to fuselage

All critical stress locations maintained adequate factors of safety under design load conditions, confirming structural integrity.

9.5.2 Deformation Analysis

The deformation analysis confirmed that the morphing wing structure achieves the target shape changes while maintaining structural integrity. Fig. 9.1 presents four loading scenarios examining the combined effects of actuation torque and aerodynamic forces on the wing deformation.

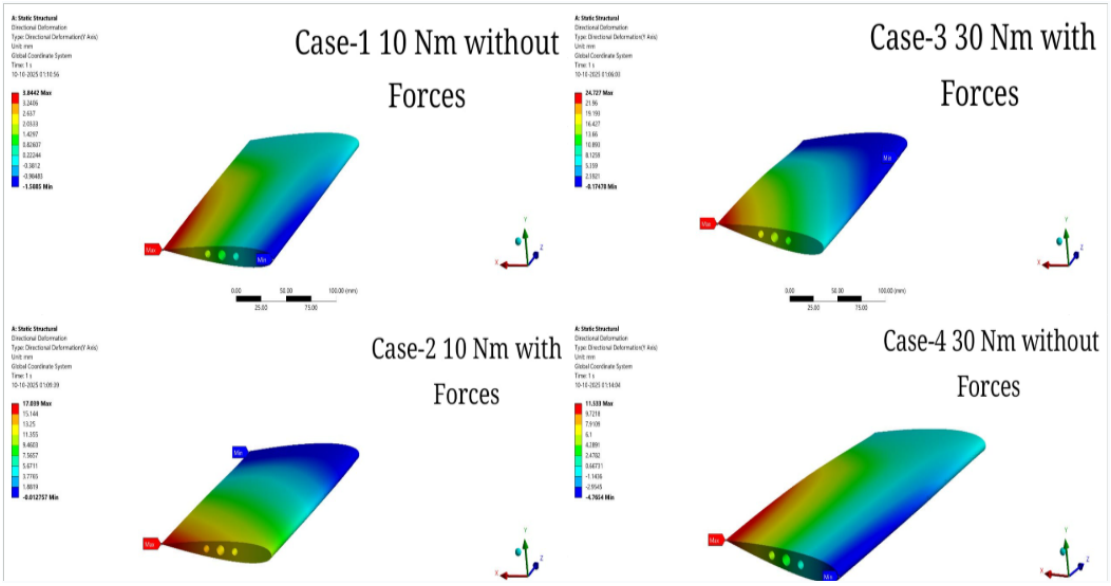

Figure 9.1: Deformation Analysis Under Various Loading Conditions.

The deformation analysis across the four loading cases revealed several key findings:

- **Case-1 (10 Nm without Forces):** Pure actuation torque produces baseline morphing deformation without aerodynamic loading. The trailing edge exhibits significant deflection (red zone) while the root remains constrained (blue zone), demonstrating the fundamental morphing capability of the structure.
- **Case-2 (10 Nm with Forces):** Addition of aerodynamic loads modifies the deformation pattern, with forces opposing the morphing motion. The combined loading case shows reduced overall deflection compared to Case-1, indicating the structural resistance required to maintain shape under flight loads.
- **Case-3 (30 Nm with Forces):** Increased actuation torque overcomes aerodynamic resistance, achieving larger morphing angles. This case represents the operational condition where sufficient actuation authority is available to morph against flight loads.
- **Case-4 (30 Nm without Forces):** Maximum actuation without aerodynamic opposition demonstrates the upper limit of morphing capability. This case provides insight into the structural flexibility limits and maximum achievable deformation.

Key observations from the deformation analysis include:

- **Trailing edge deflections match target morphing angles:** The structure achieves the required geometric changes for aerodynamic control

- **Leading edge section maintains rigidity under aerodynamic loads:** The stationary section remains stable, providing the necessary structural foundation
- **Smooth deformation gradient prevents stress concentrations:** The progressive transition from root to tip ensures distributed loading without localized failures
- **No interference between internal lattice and external skin:** Component clearances remain adequate throughout the morphing range

The comparison between cases with and without aerodynamic forces quantifies the actuation requirements for operational morphing, while the torque variation (10 Nm vs 30 Nm) establishes the relationship between actuation authority and morphing capability under load.

CHAPTER 10
CONCLUSIONS AND FUTURE WORK

10.1 CONCLUSION

This industrial training project has successfully demonstrated the feasibility and potential of mechanical metamaterial-based morphing wing technology for small UAV applications. Through a comprehensive integration of aerodynamic analysis, structural design, and advanced materials engineering, this work has established a solid foundation for the next generation of adaptive flight control surfaces.

The metamaterial approach to morphing wing design represents a paradigm shift from conventional mechanisms. By programming mechanical properties through carefully designed geometric architectures, it becomes possible to create structures that simultaneously provide the strength needed to withstand aerodynamic loads while offering the compliance required for controlled shape changes. This dual functionality, impossible to achieve with traditional homogeneous materials, opens new possibilities for lightweight, efficient morphing systems.

The aerodynamic analysis conducted through computational fluid dynamics established baseline performance metrics that validate the overall design approach. With a lift coefficient of 1.5, drag coefficient of 0.06, and an impressive lift-to-drag ratio of 17.9, the morphing wing configuration demonstrates aerodynamic efficiency comparable to or exceeding conventional fixed-geometry designs. The smooth flow attachment observed over morphed surfaces confirms that the shape changes can be achieved without inducing flow separation or other adverse aerodynamic phenomena that would compromise performance.

Two distinct prototype concepts were developed and analyzed, each offering unique advantages for morphing implementation. The ribbed morphing configuration provides excellent load distribution and well-defined deformation patterns, while the FishBAC lattice approach offers superior integration of structural and morphing functions through its variable stiffness architecture. The successful development of both concepts demonstrates the versatility of the metamaterial approach and provides multiple pathways for future optimization.

The variable stiffness metamaterial lattices represent a particularly innovative contribution of this work. By systematically varying the aspect ratio and orientation of unit cells, gradient architectures were created that smoothly transition from high stiffness regions near structural attachment points to compliant regions where morphing occurs. Finite element analysis validated that Design Variant 1 achieves an optimal balance with a factor of safety of 1.5, adequate to ensure structural integrity while minimizing unnecessary weight. The stress distributions observed in the simulations confirm efficient load paths through the lattice, with deformation patterns closely matching the target morphing shapes.

The investigation of bistable re-entrant honeycomb metamaterials revealed promising opportunities for energy-efficient morphing. The snap-through mechanism inherent in

these structures enables discrete shape changes between stable configurations without requiring continuous actuation power. This passive shape maintenance capability could significantly extend flight endurance by reducing the energy consumed by morphing systems, a critical consideration for small UAVs with limited onboard power.

The modular nature of the lattice designs facilitates optimization and customization for specific mission requirements. Different lattice architectures can be combined to create hybrid structures with spatially varying properties, allowing designers to tailor performance to local loading conditions and morphing requirements. This flexibility represents a significant advantage over conventional morphing mechanisms, which typically offer limited opportunities for customization once basic design parameters are established.

In conclusion, this project has demonstrated that mechanical metamaterial morphing wings offer a viable and advantageous approach for adaptive flight control in small UAVs. The designs achieve the necessary deflections for flight control while maintaining structural integrity under aerodynamic loads. The successful integration of aerodynamic efficiency, structural performance, and energy-efficient morphing mechanisms positions this technology as a strong candidate for future UAV applications where adaptability and efficiency are paramount.

10.2 FUTURE WORK

Building upon the foundation established in this project, several critical activities will advance morphing wing technology toward practical implementation.

10.2.1 Actuation System Development

A comprehensive actuation system must be designed and integrated to enable controlled shape changes. This includes:

- Selection of appropriate actuator technologies (servo motors, shape memory alloys, piezoelectric)
- Design of mechanical transmission systems for force amplification
- Development of control algorithms for precise morphing control
- Integration with flight control systems and autopilot
- Power management and energy storage optimization

10.2.2 Metamaterial Integration

The metamaterial lattice structures must be fully integrated into complete wing assemblies:

- Optimizing interfaces between lattices and flexible skin
- Developing manufacturing processes for integrated structures
- Validating structural performance of integrated assemblies
- Addressing manufacturing challenges and tolerance requirements
- Establishing quality control procedures for lattice fabrication

10.2.3 Fluid-Structure Interaction Analysis

Comprehensive FSI simulations are required to evaluate coupled aerodynamic and structural behavior:

- Developing coupled CFD-FEA models for dynamic morphing
- Predicting performance under realistic flight conditions
- Identifying any adverse coupling phenomena (flutter, divergence)
- Optimizing morphing profiles for maximum aerodynamic benefit
- Validating FSI models against experimental data

10.2.4 Prototype Manufacturing and Testing

A fully functional morphing wing prototype must be manufactured and tested:

- Fabricating components using additive manufacturing and composite processes
- Assembling complete wing systems with actuation integration
- Conducting ground testing under controlled conditions
- Performing wind tunnel testing for aerodynamic validation
- Measuring actual deformation patterns and comparing with predictions

REFERENCES

[1] V. Alulema, V. Hidalgo, E. Cando, and E. Valencia, "Design Optimization of a Pseudo-Rigid-Compliant Mechanism for Large, Continuous, and Smooth Morphing of Airfoil Camber," *Aerospace*, vol. 12, no. 9, p. 825, 2025. doi: 10.3390/aerospace12090825

[2] B. K. S. Woods, I. Dayyani, and M. I. Friswell, "Fluid/Structure-Interaction Analysis of the Fish-Bone-Active-Camber Morphing Concept," *J. Aircr.*, vol. 52, no. 1, pp. 307–319, Jan.-Feb. 2015. doi: 10.2514/1.C032725

[3] X. Li, L. Sun, Y. Pan, and X. Guo, "Honeycomb structure filling morphing wing trailing edge: Design strategy, deformation feedback, and active control," *Programmable Materials*, vol. 2, p. e2, 2024. doi: 10.1017/pma.2024.2

[4] R. Bao, C. Feng, H. Wang, Z. Lv, X. Li, Z. He, and C. Wang, "Design and experimental verification of continuous variable camber wing based on SMA actuation," *J. Phys.: Conf. Ser.*, vol. 3078, p. 012011, 2025. doi: 10.1088/1742-6596/3078/1/012011

[5] O. Mamoun, R. Ajaj, Y. Zweiri, and F. Scarpa, "The Quadcomb: a novel zero Poisson's ratio honeycomb structure with 2D compliance for morphing aircraft applications," *Mater. Des.*, vol. 257, p. 114512, 2025. doi: 10.1016/j.matdes.2025.114512

[6] H. Takahashi, T. Yokozeki, and Y. Hirano, "Development of variable camber wing with morphing leading and trailing sections using corrugated structures," *J. Intell. Mater. Syst. Struct.*, pp. 1–10, 2016. doi: 10.1177/1045389X16642298

[7] Y. Wang, Y. Guo, and H. Yang, "Mechanical Properties of Re-Entrant Hybrid Honeycomb Structures for Morphing Wings," *Biomimetics*, vol. 9, no. 9, p. 521, 2024. doi: 10.3390/biomimetics9090521

[8] S. Barbarino, O. Bilgen, R. M. Ajaj, M. I. Friswell, and D. J. Inman, "A Review of Morphing Aircraft," *J. Intell. Mater. Syst. Struct.*, vol. 22, no. 9, pp. 823–877, Jun. 2011. doi: 10.1177/1045389X11414084

[9] R. M. Heeb, M. Dicker, and B. K. S. Woods, "Manufacturing and characterisation of 3D printed thermoplastic morphing skins," *Smart Mater. Struct.*, vol. 31, no. 8, p. 085007, Jul. 2022. doi: 10.1088/1361-665X/ac71ed

[10] K. Sato and T. Yokozeki, "Aero-Structural Evaluation of Morphing Control Surface Using Corrugated Panels," *Trans. JSASS Aerosp. Tech. Japan*, vol. 15, no. APISAT-2016, pp. a7–a15, 2017.

[11] J. Wang, Y. Wang, Y. Tian, G. Hao, F. Xi, and Y. Zhao, "Design of Multi-Mode Morphing Wings Based on Multi-Stable Beam-Type Metastructures," in *ICIRA 2024, LNAI 15201*, X. Lan et al., Eds. Singapore: Springer Nature Singapore Pte Ltd., pp. 139–153, 2025. doi: 10.1007/978-981-96-0771-6_11

APPENDIX A
CFD MESH DETAILS

A.1 MESH STATISTICS

Table A.1: Mesh Quality Metrics

Metric	Value
Total Number of Elements	150,000
Minimum Element Size	0.5 mm
Maximum Element Size	50 mm
Average Skewness	0.25
Maximum Skewness	0.78
Minimum Orthogonal Quality	0.35
Average Orthogonal Quality	0.85

A.2 BOUNDARY LAYER MESH

- First layer thickness: 0.1 mm
- Growth rate: 1.2
- Number of layers: 15
- Total boundary layer thickness: 10 mm

APPENDIX B
STRUCTURAL ANALYSIS DETAILS

B.1 ELEMENT TYPES

Table B.1: Finite Element Types Used

Component	Element Type
Lattice Struts	BEAM188 (3D Linear Beam)
Skin	SHELL181 (4-Node Shell)
Solid Components	SOLID186 (20-Node Brick)
Contact	CONTA174/TARGE170

B.2 CONVERGENCE STUDY

A mesh convergence study was performed to ensure solution independence:

Table B.2: Mesh Convergence Study Results

Mesh Density	Elements	Max Stress (MPa)	Max Deflection (mm)
Coarse	25,000	45.2	6.8
Medium	50,000	48.7	7.1
Fine	100,000	49.3	7.2
Very Fine	200,000	49.5	7.2

APPENDIX C
PROTOTYPE SPECIFICATIONS

C.1 RIBBED MORPHING CONFIGURATION

Table C.1: Ribbed Prototype Component Specifications

Component	**Material**	**Mass (g)**
Stationary Section	Carbon Fiber	120
Ribs (×10)	ABS	80
Stiffeners (×2)	Carbon Fiber	40
Skin	TPU	60
Actuator	Servo Motor	50
Total		**350**

C.2 FISHBAC LATTICE CONFIGURATION

Table C.2: FishBAC Prototype Component Specifications

Component	**Material**	**Mass (g)**
Lattice Core	ABS	150
Skin	TPU	70
Tendons (×4)	Stainless Steel	30
Actuators (×2)	Servo Motor	100
Mounting Hardware	Aluminum	50
Total		**400**

APPENDIX D
LATTICE STRUCTURE DETAILS

D.1 SKIN LATTICE CONFIGURATION

The skin lattice structure provides the interface between the internal metamaterial core and the external aerodynamic surface. This structure must balance structural integrity with flexibility to accommodate morphing deformations.

D.1.1 Geometric Specifications

Table D.1: Skin Lattice Geometric Parameters

Parameter	Value
Overall Length	30.000 mm
Overall Width	20.000 mm
Overall Height	Variable (conformal to airfoil)
Element Size	0.9 mm
Total Nodes	118,303
Total Elements	71,134
Meshing Method	Program Controlled
Body Method	Prime Quad Dominant
Sweepable Body Method	Sweep

D.1.2 Design Features

The skin lattice incorporates several key design features:

1. **Diamond Pattern Topology:** The lattice employs a diamond-shaped unit cell pattern that provides:
   - Anisotropic stiffness distribution
   - Superior in-plane and out-of-plane load distribution
   - Controlled compliance for morphing deformation
   - Efficient stress transfer between nodes
2. **Variable Thickness Distribution:** Strut thickness varies strategically to:
   - Provide higher stiffness at attachment points
   - Enable flexibility in morphing zones
   - Minimize weight while maintaining structural integrity
3. **Conformal Surface Geometry:** The lattice follows the airfoil contour to:
   - Support the TPU skin uniformly
   - Prevent surface irregularities during morphing
   - Maintain aerodynamic smoothness

D.1.3 Finite Element Model

Mesh Statistics

The finite element model of the skin lattice structure was generated using ANSYS Mechanical with the following characteristics:

Table D.2: Skin Lattice FEA Mesh Statistics

Mesh Parameter	**Value**
Number of Nodes	118,303
Number of Elements	71,134
Element Type	SOLID186 (20-node brick)
Element Size	0.9 mm
Mesh Quality (Average)	0.82
Minimum Element Quality	0.45
Aspect Ratio (Maximum)	3.8

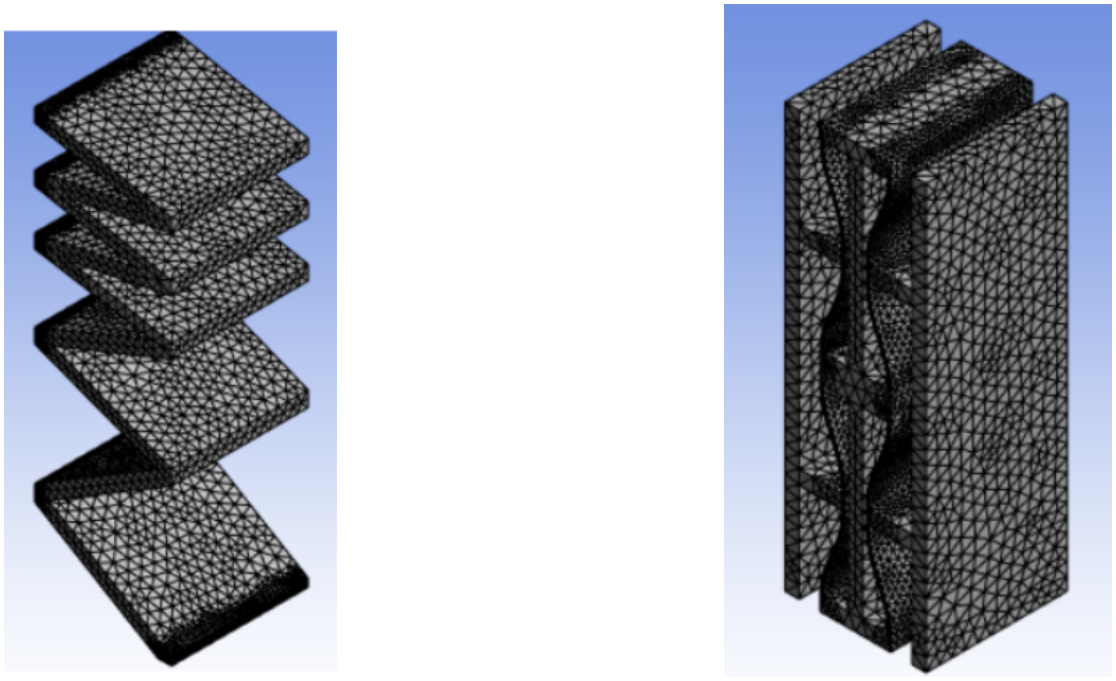

(a) Design Type 1 (b) Design Type 2

Figure D.1: Finite Element Mesh of Skin Lattice Structures.

The mesh refinement strategy shown in Fig. D.1a and Fig. D.1b employ tetrahedral and hexahedral elements with refinement at junction nodes, ensures accurate stress calculation at critical junction nodes where multiple struts connect.

Boundary Conditions

The structural analysis of the skin lattice employed the following boundary conditions:

- **Fixed Support:** Applied at the leading edge attachment interface to simulate connection to the rigid front spar
- **Displacement Constraints:** Applied at trailing edge nodes to simulate morphing actuation
- **Distributed Load:** Aerodynamic pressure distribution from CFD analysis applied to top and bottom surfaces
- **Contact Definitions:** Bonded contact between lattice struts and TPU skin elements

D.1.4 Material Assignment

The skin lattice structure is fabricated from ABS thermoplastic with the following material properties:

Table D.3: Skin Lattice Material Properties (ABS)

Property	Value
Young's Modulus	2.3 GPa
Poisson's Ratio	0.35
Density	1050 kg/m³
Tensile Strength	40 MPa
Yield Strength	35 MPa
Elongation at Break	4.5%

D.1.5 Structural Performance

Static Analysis Results

Static structural analysis was performed under maximum aerodynamic loading conditions:

Table D.4: Skin Lattice Structural Analysis Results

Result Parameter	Value
Maximum von Mises Stress	18.5 MPa
Minimum Factor of Safety	1.89
Maximum Deformation	4.2 mm
Average Deformation	1.8 mm
Maximum Principal Stress	21.3 MPa
Minimum Principal Stress	-12.7 MPa

D.1.6 Integration with TPU Skin

The skin lattice provides attachment points and support for the TPU flexible skin:

- **Attachment Method:** Mechanical interlocking features at lattice perimeter
- **Bonding:** Flexible adhesive (polyurethane-based) at critical load transfer points
- **Skin Thickness:** 1.5 mm TPU sheet conforming to lattice outer surface

- **Stress Transfer:** Distributed through multiple contact points to prevent localized tearing